The American Society of Mechanical Engineers

Reprinted From
Proceedings of the ASME/JSME Thermal Engineering
Editors: L. S. Fletcher, and T. Aihara
Book No. H0933A – 1995

NUMERICAL ANALYSIS OF TURBULENT STRUCTURE AND HEAT TRANSFER IN A SQUARE DUCT WITH ONE ROUGH WALL

Hitoshi SUGIYAMA, Mitsunobu AKIYAMA
Department of Mechanical Systems Engineering,
Utsunomiya University,
Utsunomiya, Tochigi
Japan

Masashi MATSUMOTO
Nissan Motor Co., Ltd.,
Musashimurayama, Tokyo
Japan

ABSTRACT

A numerical analysis of heat transfer has been performed for fully developed turbulent flow in a straight square duct with one roughened wall by using algebraic Reynolds stress model and turbulent heat flux model. Considering preciously anisotropy of turbulence for temperature field as well as the flow field, the turbulent heat flux model, in which model convection and diffusion terms are simplified as an algebraic expression of turbulent heat flux by means of Rodi's approximation, is adopted in this calculation. The calculated results were compared with the experimental data available presented by Hirota et al. As is well known in a square duct with smooth walls, a pair of vortices is observed in a quadrant of the duct cross section. But the experimental data of a roughened wall revealed formation of only one vortex in a half cross section in a square duct with one roughened wall. The present method can predict well this large eddy caused by the secondary flow of the second kind in a half cross section and a small eddy is observed in the upper wall corner region. Additionally in the both results, the contour lines of temperature are distorted in the upper region of square duct by the secondary flow. The production terms of turbulent heat flux $\overline{u_3 T'}$, which plays an important role in the heat transfer near the roughened wall region, are compared with the experimental data. The present method is able to predict the distribution of this terms near the roughened wall.

NOMENCLATURE

a	:	thermal diffusivity
D_h	:	hydraulic diameter
P_k	:	production term of turbulent energy equation
k	:	turbulence kinetic energy
L	:	length scale of turbulence
Re	:	Reynolds number
T	:	mean temperature
T'	:	fluctuating temperature
u_i	:	fluctuating velocity
U_i	:	mean velocity
U_b	:	bulk velocity
ε	:	dissipation of turbulent energy
ν	:	kinematic viscosity
π_{ij}	:	pressure–strain correlation
π_{iT}	:	pressure–temperature gradient correlation
ρ	:	density

INTRODUCTION

It has been well known that turbulent flows in non–circular ducts are accompanied by secondary flows of the second kind termed by Prandtl. The secondary flow of this type is attributable to the presence of Reynolds–stress gradients across the cross–sectional plane. Although this secondary velocity is only of the order of two or three percent of the streamwise bulk velocity, its presence displaces the lines of constant axial velocity considerably toward the corners of the duct, yielding a relatively high velocity field there. On the other hand, from a thermal engineering point of view, non–circular cross section shapes with roughened walls are often encountered in engineering practice to enhance the convective heat transfer by promoting turbulence. It can be easily expect that the temperature distribution and secondary flow pattern are influenced by roughened walls in a non–circular duct. Therefore, in a non–circular duct with rough walls, an understanding of the characteristics of the secondary flow is indispensable for clarifying the effects of rough walls on turbulent convective heat transfer and for developing augmentation technique of heat

transfer.

In experimental study, very little has been reported (Launder and Ying,1972, Humphrey and Whitelaw,1980) about influence of rough walls on secondary flow behavior. However, Fujita et al.(1989) have reported systematically about the turbulent flow in non-circular duct with rough walls. They have measured accurately Reynolds stresses and secondary flow pattern in a square duct with roughened walls on opposite sides (Yokosawa et al.,1989) and with one roughened wall (Fujita et al.,1986) as an object of experimental research. And they have concluded that the distributions of mean flow velocity, Reynolds stresses and secondary flow are very different from that in non-circular duct with smooth walls. Moreover, Hirota et al.(1992) presents experimental results about a mean temperature field in forced convective heat transfer for a turbulent flow through a square duct with a roughened wall. They have examined the mechanism of heat transfer enhancement by the rough wall, considering the transport equations of Reynolds stress and turbulent heat flux.

In this type of numerical analysis, a few reports concerned with roughened wall have presented as well as experimental research. Hanjalic and Launder(1972) have calculated for the asymmetric flow introduced by fixing ribs of square cross-section aligned vertically to the flow and pitched 10 rib heights apart to one wall. But their numerical analysis has been carried out for two dimensional turbulent flow without predicting the secondary flow of the second kind. Calculation of Demuren and Rodi (1984) were carried out for the fully developed turbulent flow in a 5:1 ratio rectangular channel with a roughened wall studied experimentally by Hinze(1973). Calculation results displayed the distortion of primary velocity contours, distribution of turbulent shear stress and kinetic energy along wall bisector. The calculation reported by Fujita et al.(1988) was performed in a square duct with two roughened facing walls with k and ε model coupled to the algebraic stress model developed by Launder and Ying(1973). Though they could predict the velocity vector of secondary flow, it seemed that calculated flow pattern was slightly different from the experimental data measured by Fujita et al.(1989). Sugiyama et al.(1993) also carried out numerical analysis in a square duct with two roughened facing walls by algebraic Reynolds stress model (Sugiyama et al.,1991) that is different from Launder and Ying(1973) model. The calculated results are in good agreement with the experimental data and display more reasonable consequence than the calculated results of Fujita et al.(1988). On the contrary to the numerical analysis of flow field, it seems that there are few numerical results concerned with heat transfer in non-circular duct with roughened walls.

Considering these researches of duct flow with rough walls, the purpose of this present research is to predict numerically turbulent heat transfer in a square duct of fully developed flow field that has been measured by Hirota et al.(1992) by means of algebraic Reynolds stress model and turbulent heat flux model.

TECHNIQUE OF ANALYSIS

Subject of numerical analysis

As the subject of numerical analysis, we have adopted the experimental data for the fully developed turbulent flow in a square duct with one roughened wall presented by Hirota et al. (1992). Fig.1 shows the orthogonal coordinate system set in duct and a schematic diagram of the experimental apparatus. The experimental duct has a 50 mm square cross section and is 4770 mm in length. The duct includes a heating part that has a structure of a double-duct and is between the duct exit and 1750 mm upstream from the exit. The experiments were conducted under the conditions of constant wall temperature. Roughness elements whose cross-section was 1 mm square were located at 10 mm intervals, transverse to the primary flow, to make up the one roughened wall of the duct. Reynolds number $Re=U_b D_h / \nu$, where U_b is the bulk velocity, D_h is hydraulic diameter and ν is the kinematic viscosity of air, was set to be 6.5×10^4. Measurements were conducted at the cross section 100 mm upstream from the duct exit, which is $93.4D_h$ downstream from the duct entrance and $33D_h$ downstream from the heating part entrance, by using a hot wire anemometer.

The transport equation for Reynolds stresses

The anisotropy nature of the turbulence was expressed by the Reynolds stress equations. Nevertheless, an analysis conserving the accuracy of these equations is not possible so that some modeling effort was required. The set of differential equations governing the transport of the Reynolds stresses are derived from the Navier-Stokes equation,

$$\frac{D\overline{u_iu_j}}{Dt} = -\left(\overline{u_iu_k}\frac{\partial U_j}{\partial x_k} + \overline{u_ju_k}\frac{\partial U_i}{\partial x_k}\right) + \overline{\frac{p}{\rho}\left(\frac{\partial u_i}{\partial x_j} + \frac{\partial u_j}{\partial x_i}\right)} - \frac{\partial}{\partial x_k}\left[\overline{u_iu_ju_k} - \nu\frac{\partial \overline{u_iu_j}}{\partial x_k} - \overline{\frac{p}{\rho}(\delta_{jk}u_i + \delta_{ik}u_j)}\right] - 2\nu\overline{\frac{\partial u_i}{\partial x_k}\frac{\partial u_j}{\partial x_k}} \quad (1)$$

The first term of the right hand side is the production term P_{ij}, the second term is the pressure strain correlation π_{ij}, the third term is the diffusion term , and forth term is the dissipation term ε_{ij}. To get the solution of the Reynolds stress equation in the form presented above is difficult. It is necessary to introduce model assumptions for the correlations appearing in the exact equation. As for the modeling of the convective term and of the diffusion term, the approximation by

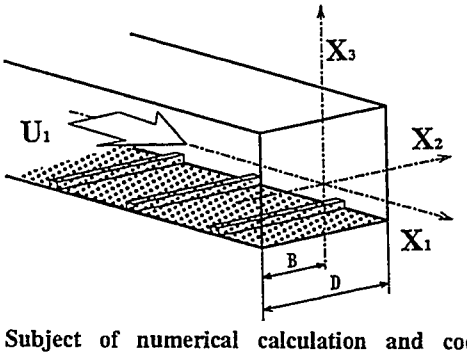

Fig.1 Subject of numerical calculation and coordinate system

Rodi(1976) was employed. By Rodi's approximation,these terms expressed in a differential form for Reynolds stress component can be transformed into the algebraic equation. In the Reynolds stress model equation, a particularly problematic task is the modeling of the pressure–strain correlation term that is also defined redistribution term. Following Chou(1945),the pressure–strain term can be expressed precisely. Chou suggests that there are two distinct kinds of interaction giving rise to the correlation between fluctuating pressure and fluctuating velocity of strain; one involving just fluctuating quantities $\pi_{ij,1}$ and another arising from the presence of the mean rate of strain $\pi_{ij,2}$. In the present model, we adopted the Rotta's linear return–to–isotropy model as the interaction of fluctuating velocity. Rotta's proposal for $\pi_{ij,1}$ may be written as shown in Table 1. In Table 1, c_1 of $\pi_{ij,1}$ represents empirical constant.

For $\pi_{ij,2}$ the correlation can be approximated in the form:

$$\pi_{ij,2} = \left(\frac{\partial U_l}{\partial x_m}\right) a_{lj}^{mi} \tag{2}$$

and a_{lj}^{mi} is the forth–order tensor. The forth–order tensor is determined by following kinematic constraints:

$$a_{lj}^{mi} = a_{lj}^{im} = a_{jl}^{im} \tag{3}$$

$$a_{li}^{mi}\frac{\partial U_l}{\partial x_m} = 0 \tag{4}$$

$$a_{jj}^{mi} = 2\overline{u_m u_i} \tag{5}$$

These constraints are different from Rotta's proposal constraints in refer to the form of Eq.(4). We adopted the above constraints for the reason that $\pi_{ij,2}$ is defined as the products between the forth order tensor and mean strain as shown in Eq.(2). The constraints in the form of Eqs.(3), (4) and (5) arise from symmetry, mass conservation and Green's theorem, respectively. The form of Eq.(5) suggests that the forth–order tensor might be approximated by linear combination of Reynolds stresses. The most general such tensor satisfying the symmetry constraints implied by Eq.(5) may be written as:

$$\begin{aligned} a_{lj}^{mi} = {} & \alpha\delta_{lj}\overline{u_m u_i} + \beta(\delta_{ml}\overline{u_i u_j} + \delta_{mj}\overline{u_i u_l} + \delta_{il}\overline{u_m u_j} + \delta_{ij}\overline{u_m u_l}) \\ & + c_2\delta_{mi}\overline{u_l u_j} + \{\eta\delta_{mi}\delta_{lj} + \upsilon(\delta_{ml}\delta_{ij} + \delta_{mj}\delta_{il})\}k \end{aligned} \tag{6}$$

which is indicated by Launder, Reece, and Rodi(1975). δ_{ij} represents Kronecker delta and c_2, α, β, η, υ are empirical constants. The application of Eqs.(4) and (5) enables two constants of Eq.(6) to be expressed in terms of c_2. On combining Eqs.(2) and (6), the complete influence of the mean strain on the pressure–strain correlation may be expressed in Table 1. In Table 1, ζ is independent constant determined by experimental data and α and β of Eq.(6) are defined as a function of c_2. On the other hand, in Launder, Reece and Rodi model, ζ, α and β are defined as a only function of c_2. Therefore, in the present model, we can take account of more experimental data than Launder, Reece and Rodi.

The wall effect term $\pi_{ij,w}$ on turbulent stresses, which will be negligible away from the vicinity of a solid boundary, is expressed in this model by making the empirical constants as a

Table 1 Pressure–strain correlations

$\pi_{ij,1} + \pi_{ji,1}$	$-c_1 \cdot \frac{\epsilon}{k}\left(\overline{u_i u_j} - \frac{2}{3}k\delta_{ij}\right)$
$\pi_{ij,2} + \pi_{ji,2}$	$-\frac{c_2+8}{11}\left(P_{ij} - \frac{2}{3}P_k\delta_{ij}\right)$ $+\zeta k\left(\frac{\partial U_i}{\partial x_j} + \frac{\partial U_j}{\partial x_i}\right) - \frac{8c_2-2}{11}\left(D_{ij} - \frac{2}{3}P_k\delta_{ij}\right)$
$[\pi_{ij} + \pi_{ji}]_w$	$c_1 = c_1^* + c_1' \cdot f\left(\frac{L}{X_w}\right)$, $c_2 = c_2^* + c_2' \cdot f\left(\frac{L}{X_w}\right)$, $\zeta = \zeta^* + \zeta' \cdot f\left(\frac{L}{X_w}\right)$

$P_{ij} = -\overline{u_i u_k}\frac{\partial U_j}{\partial x_k} - \overline{u_j u_k}\frac{\partial U_i}{\partial x_k}$, $\quad D_{ij} = -\overline{u_i u_k}\frac{\partial U_k}{\partial x_j} - \overline{u_j u_k}\frac{\partial U_k}{\partial x_i}$

$P_k = -\overline{u_k u_l}\frac{\partial U_k}{\partial x_l}$

Table 2 Constants in pressure–strain correlations

c_1^*	c_2^*	ζ^*	c_1'	c_2'	ζ'
1.40	0.44	-0.16	-0.35	0.12	-0.10

function of dimensionless distance from the wall. This wall effect term used in this analysis is summarized in Table 1. In wall effect term, $f(L/X_w)$ is a function of the dimensionless wall distance. It expresses the influence of the wall and takes the value 1 in its vicinity, approaching 0 in with the increasing distance of it. X_w expresses the distance from the wall and L defined length scale of turbulence.

The values of constants have been chosen such that, when f=0, the model yields the correct Reynolds stress components for nearly homogeneous shear flow of Champangne, Harris and Corrsin(1970), and, when f=1, the relative magnitude of the stress components agrees with a consensus of near wall turbulence. Moreover, we have used the experimental data of Harris, Graham and Corrsin(1977) who reported further homogeneous shear flow data where the strain rate was higher than that of Champagne, Harris and Corrsin. The constants used in this pressure–strain term are noted in the Table 2.

The forth term of Eq.(1) is the homogeneous part of dissipation. This term is modeled commonly with the assumption of the isotropic motion for the dissipation, namely:

$$\epsilon_{ij} = 2\nu\overline{\frac{\partial u_i}{\partial x_k}\frac{\partial u_j}{\partial x_k}} = \frac{2}{3}\delta_{ij}\epsilon \tag{7}$$

<u>The transport equation for turbulent heat fluxes</u>

The equations governing the transport of heat flux in turbulent field may be written as (when the buoyancy effect and viscous diffusion term are neglected)

$$\begin{aligned} \frac{D\overline{u_i T'}}{Dt} = {} & -\left(\overline{u_i u_j}\frac{\partial T}{\partial x_j} + \overline{u_j T'}\frac{U_i}{\partial x_j}\right) + \overline{\frac{p}{\rho}\frac{\partial T'}{\partial x_i}} \\ & - \frac{\partial}{\partial x_j}\left(\overline{u_i u_j T'} + \overline{\frac{p}{\rho}T'\delta_{ij}}\right) - (\nu + a)\overline{\frac{\partial T'}{\partial x_j}\frac{\partial u_i}{\partial x_j}} \end{aligned} \tag{8}$$

where T and T' denote mean and fluctuating temperatures, ρ the mean fluid density, p the instantaneous pressure fluctuation about its mean value. The equation is solved simultaneously with the transport equations for Reynolds stresses. Before these equations are applied for temperature field, unknown correlations in Eq.(8) must be approximated in

terms of the mean field distributions of velocity, temperature, the Reynolds stresses, the turbulent fluxes, and the characteristic time scale.

The transport terms in Eq.(8) are approximated by Rodi's proposal as:

$$\frac{D\overline{u_iT'}}{Dt} - Diff_{iT} = \frac{\overline{u_iT'}}{2k}(P_k - \epsilon) + \frac{\overline{u_iT'}}{2\overline{T'^2}}(P_T - \epsilon_T) \qquad (9)$$

where D_{iT}, P_T and ε_T denote diffusion term of Eq.(8), the rate of production and destruction of the temperature fluctuations, respectively. In this calculation, it is assumed that the rate of production P_T is equal to the destruction ε_T. The pressure–temperature gradient correlation is the counterpart of the pressure–strain term in the Reynolds stress equations. In the parallel with the pressure–strain term, the pressure–temperature gradient correlation consists of a turbulence interaction part $\pi_{iT,1}$, a mean–strain part $\pi_{iT,2}$ and wall effect part $\pi_{iT,w}$. The turbulence interaction part proposed by Lumley (1975) and the mean–strain part presented by Launder(1975) are approximated as shown in Table 3. Wall effect part is expressed in the same way as the Reynolds stress equations. The wall effect part is also summarized in Table 3.

The forth term of the right hand side of Eq.(8) represents the viscous destruction. As the viscous destruction is zero in the local isotropic turbulence, it will be negligible at high Reynolds number. The mean field production term that is the first term of the right hand side of Eq.(8) needs no approximation, since it contains only second moments and the mean field variables.

The values of constants of the transport equations of turbulent heat flux are determined using the experimental data of turbulent Prandtl number in homogeneous turbulent shear flow and near wall turbulence. The values of constants are shown in Table 4.

Method of numerical analysis

A control volume method was adopted with applying the staggered mesh expression for uniform grid points. As a result of using staggered mesh, Reynolds stresses vector and scalar parameters on the staggered mesh are located at control –volume faces and grid points, respectively. In order to discretize the convection terms, we employed quadratic interpolation (QUICK) for the momentum equations and power law interpolation (PLDS) for the transport equations of turbulent energy and dissipation. The SIMPLE algorithm, which stands for semi–implicit method for pressure linked equation, was used to solve pressure correction and velocity correction. In calculation for developing turbulent flow,inlet length is 102.8 hydraulic diameter long. Computation was performed with 12x22 uniform mesh over the half of the duct cross section, 120 mesh along the streamwise and 6.5×10^4 for the Reynolds number.

In the experimental apparatus, bottom wall of duct was roughened over its length by attaching transversely 1 mm square sectioned brass roughness element at 10 mm intervals. On the other hand, the calculation was done by using the wall function method as a boundary condition of turbulent energy and dissipation without considering the figure of roughness element. The universal law of the wall and local equilibrium condition, which can be applied to the near wall region, are used as a boundary condition for turbulent energy and dissipation. As the boundary condition of roughened wall in this case, Fujita et al.(1988) find out following empirical equation:

$$\frac{U_l}{U_\tau} = \frac{1}{0.42} ln\left(\frac{U_\tau y}{\nu}\right) - 8.4 \qquad (10)$$

where U_τ represents friction velocity. In this numerical calculation, the above log law of the rough wall is adopted as boundary condition for turbulent energy and dissipation. In the case of smooth walls, standard log law is used as a boundary condition for turbulent energy and dissipation. And constant temperature is set at all walls as well as the experiment.

Table 3 Pressure–temperature gradient correlations

$\pi_{iT,1}$	$-c_{1T}\cdot\frac{\varepsilon}{k}\overline{u_iT'} - c'_{1T}\cdot\frac{\varepsilon}{k}k\left(\frac{\overline{u_iu_j}}{k}-\frac{2}{3}\delta_{ij}\right)\overline{u_jT'}$
$\pi_{iT,2}$	$c_{2T}\cdot\overline{u_jT'}\frac{\partial U_i}{\partial x_j} - c'_{2T}\cdot\overline{u_jT'}\frac{\partial U_j}{\partial x_i}$
$\pi_{iT,w}$	$c_{1T} = c^*_{1T}\left\{1 + c_{1T,w}\cdot f\left(\frac{L}{X_w}\right)\right\}$, $c'_{1T} = c'^*_{1T}\left\{1 + c_{1T,w}\cdot f\left(\frac{L}{X_w}\right)\right\}$, $c_{2T} = c^*_{2T}\left\{1 + c_{2T,w}\cdot f\left(\frac{L}{X_w}\right)\right\}$, $c'_{2T} = c'^*_{2T}\left\{1 + c_{2T,w}\cdot f\left(\frac{L}{X_w}\right)\right\}$

Table 4 Constants in pressure–temperature correlations

c^*_{1T}	c'^*_{1T}	c^*_{2T}	c'^*_{2T}	$c_{1T,w}$	$c_{2T,w}$
3.9	-2.5	0.8	0.2	0.25	-0.46

RESULTS AND DISCUSSIONS

Comparison for mean flow field

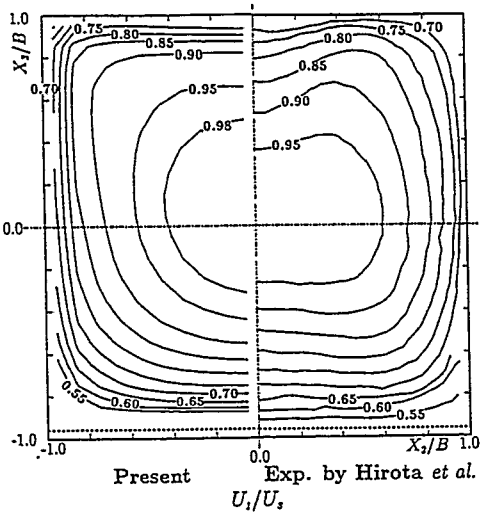

Fig.2 Comparison of axial mean velocity

The contours of primary flow velocity U_1 calculated and measured are shown in the left- and right-hand sections, respectively, of Fig.2. The broken line drawn near the bottom shows the roughness height. The numbers in the figure represent the velocities normalized by the maximum primary flow velocity U_e. The calculated results correspond to the location $93.3D_h$ as well as the experimental data. In both results, the contours become very concave near the top smooth wall and are almost parallel to the wall near the rough wall. The fast flowing fluid is observed near the top and side smooth wall in the experimental data, since the resistance to flow induced by rough wall is larger than that of smooth wall. The calculated results predict also this characteristic phenomenon and are in good agreement with the experimental data except for the central region of the square duct.

The comparison the secondary flow velocity distributions of calculation with the experimental result are shown in Fig.3 with vectors. As is well known, in the smooth duct, a pair of contrarotating longitudinal vortices exists in each quadrant of the duct cross section. On the other hand, in the rough square duct, large longitudinal vortex appears in half of the cross section. The present method can predict well this large eddy caused by the secondary flow of the second kind in a half cross section and a small eddy is observed in the upper wall corner region. However, a small eddy that appeared in the calculated results is not recognized clearly in the experimental data as shown in Fig.3. In the core duct, secondary currents proceed downward from the top smooth wall to the bottom rough wall along the duct mid plane. Although the calculation can not predict preciously the central location of vortex, the calculated results are able to estimate the characteristic feature of the secondary flow.

The distributions of the wall shear stress and wall heat flux along the top smooth wall are shown in Fig.4. These parameters are normalized by averaged wall shear stress and averaged wall heat flux obtained by integrating over the top smooth wall. In experimental data, it is pointed out that the distribution of wall shear stress is similar to that of wall heat flux and these two profiles show the maximum value at $X_3/B=0.5$. Judging from the comparison of these characteristic features, it seems that the present method is in good agreement with the experimental data.

Fig.5 shows the distributions of the wall shear stress and wall heat flux along the side smooth wall. As to profile of wall heat flux, the calculated result coincides with the experimental data and the maximum value is located negative sign region of X_3 coordinate in both results. On the other hand, the discrepancy between experimental wall shear stress and calculated one is observed in positive sign region of X_3 coordinate.

Comparison for mean temperature field

Fig.6 presents the distributions of temperature in the duct cross section. The contour maps are similar in shape to those of U_1 presented in Fig. 2. T_e and T_w stand for the value of

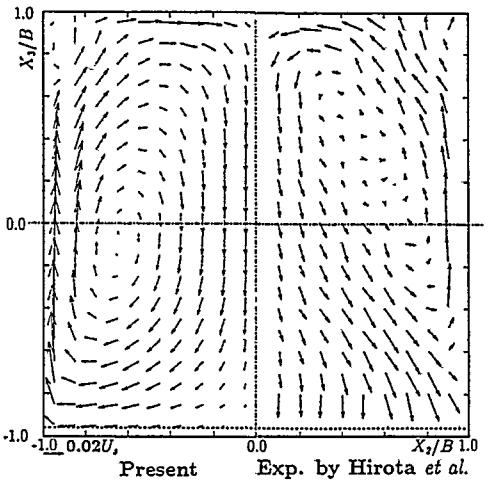

Fig.3 Comparison of secondary flow

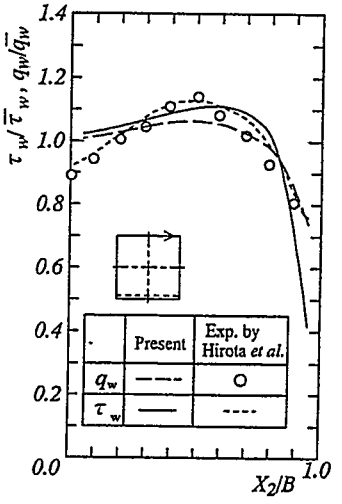

Fig.4 Comparison of wall shear stress and wall heat flux along the top smooth wall

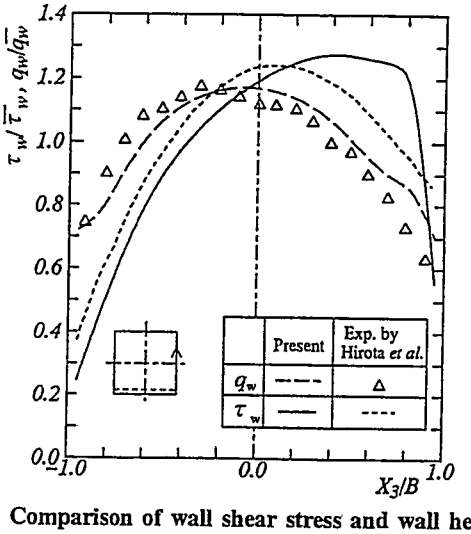

Fig.5 Comparison of wall shear stress and wall heat flux along the side smooth wall

temperature at the center of duct and that on the wall, respectively. The distorted contours near the top smooth wall are caused by the secondary flow proceeded downward from the top smooth wall to the bottom rough wall along X_3 coordinate. If one compares the calculated results presented by using turbulent heat flux model with experiment data, it seems that agreement is good.

To examine precisely the similarity between the distribution of temperature and that of axial mean velocity, plots of U_1 / U_s versus Θ / Θ_s are evaluated from both results near the region of smooth wall and rough wall, where Θ stands for the mean temperature difference between the fluid and the wall and Θ_s the value of Θ at the center of duct. These plotted results of near the smooth wall and the rough wall are shown in Fig.7(a) and Fig.7(b), respectively. In these figures, perfect similarity between these parameters means that plot of U_1 / U_s versus Θ / Θ_s is fixed along the 45 degree line. As shown in Fig.7(a), the experimental result indicates stronger similarity than the calculated results, judging from that plots of the experiment are located near the 45 degree line. In calculation, clearly weak similarity is observed. This weak similarity is most likely caused by the difference between the distorted contours of the axial mean velocity and that of temperature near the top smooth wall. The contour of axial velocity, as shown in Fig.2, is not so distorted as that of temperature. On the other hand, both the experiment and the calculation suggest that the similarity near the rough wall is weak as shown in Fig.7(b). As to similarity near the rough wall, the calculation agrees well with the experiment.

Fig.8 shows the comparison with the experimental distributions of local Nusselt number over the top smooth wall and the side smooth wall. Although the calculation underestimates the value of local Nusselt number over both the top and side smooth wall, the location of maximum value and distributions with convex curve coincides with the experimental data.

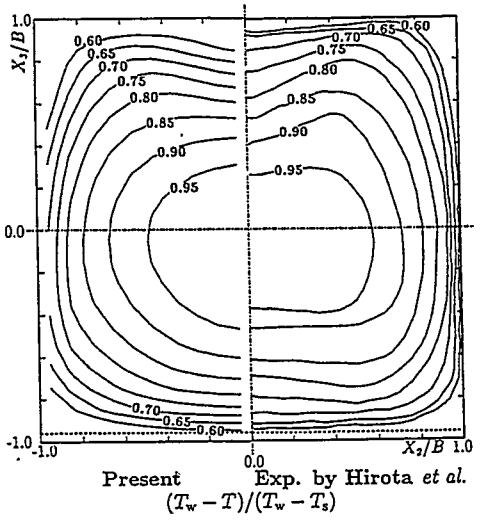

Fig.6 Comparison of mean temperature

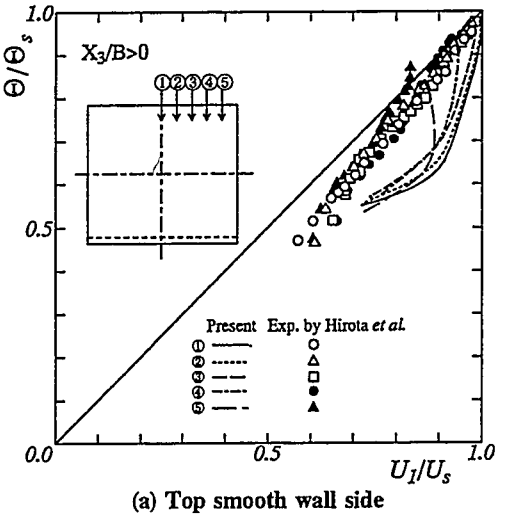

(a) Top smooth wall side

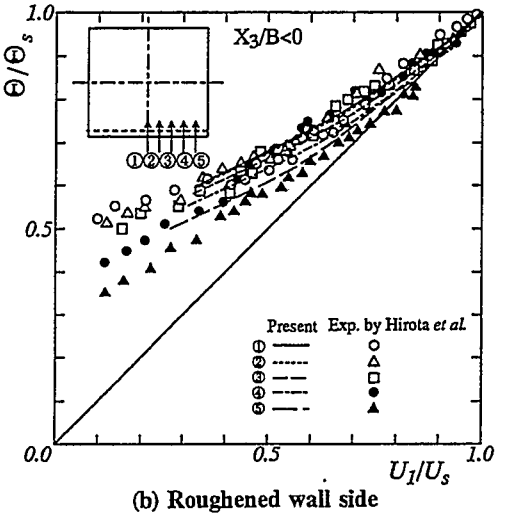

(b) Roughened wall side

Fig.7 Comparison of similarity between axial mean velocity and mean temperature

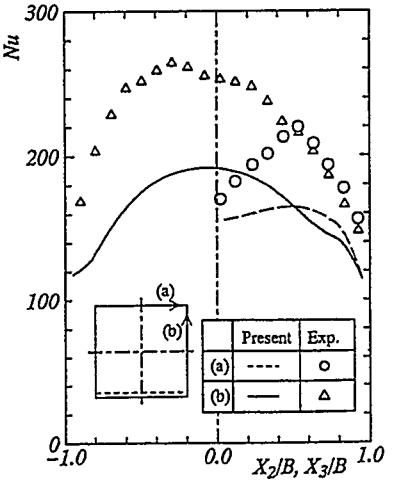

Fig.8 Comparison of local Nusselt number

Heat transfer near rough wall is intimately bound up with turbulent heat flux $\overline{u_3T'}$. The production term of $\overline{u_3T'}$ can be expressed by following relation:

$$P_{3T} = -\left(\overline{u_3^2}\frac{\partial T}{\partial x_3} + \overline{u_3T'}\frac{\partial U_3}{\partial x_3} + \overline{u_1u_3}\frac{\partial T}{\partial x_1} + \overline{u_1T'}\frac{\partial U_3}{\partial x_1}\right)\frac{D_h}{U_b^2\Theta_b} \quad (11)$$

In the above equation, the first, second, third and forth term of right hand side denotes as PH1, PH2, PH3 and PH4, respectively. For the fully developed turbulent flow, PH3 and PH4 are equal to zero. Fig.9 shows calculated result of PH1 and PH2 and the experimental result of PH1. The calculation can predict well the experimental distribution of the production first term of $\overline{u_3T'}$ and suggests that the first term plays an important role in producing turbulent heat flux $\overline{u_3T'}$.

The similarity between the turbulent heat flux and the Reynolds stress, which is called Reynolds' analogy, is examined in calculated results. Reynolds stresses $\overline{u_1^2}$, $\overline{u_1u_2}$ and $\overline{u_1u_3}$ generated by momentum transfer correspond to the turbulent heat flux $\overline{u_1T'}$, $\overline{u_2T'}$ and $\overline{u_3T'}$ in temperature field, respectively. Figs.10(a), (b) and (c) show the comparison of the contours of turbulent heat flux $\overline{u_1T'}$, $\overline{u_2T'}$ and $\overline{u_3T'}$ with that of correspond Reynolds stresses, respectively. In Fig.10(a), it is pointed out as characteristic phenomenon that the maximum absolute value of turbulent heat flux $\overline{u_1T'}$ and Reynolds stress $\overline{u_1^2}$ exists near rough wall and decays gradually toward the center of duct cross section. Although the value of turbulent flux is different from that of Reynolds stress, the weak similarity between the distribution of turbulent heat flux and that of Reynolds stress is observed. Moreover, as shown in Fig.10(b), the maximum value of the turbulent heat flux $\overline{u_2T'}$ is observed at corner region of rough wall side as well as the Reynolds stress $\overline{u_1u_2}$ and zero value line near the top smooth wall side is

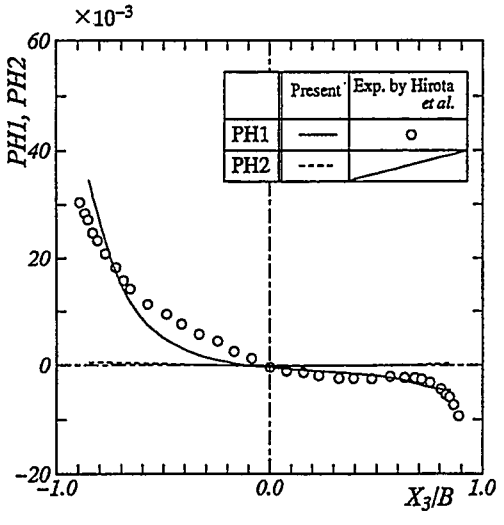

Fig.9 Comparison of production term for turbulent heat flux $\overline{u_3T'}$

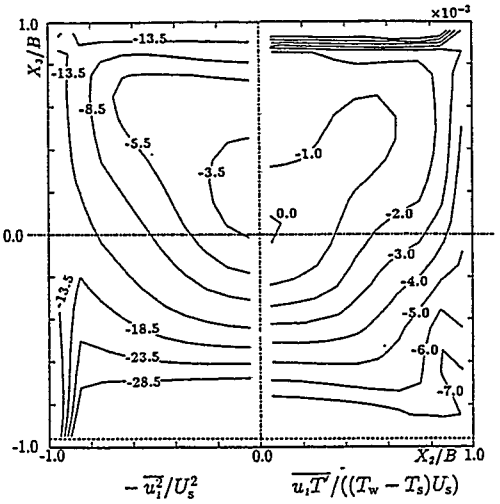

(a) Distribution of $\overline{u_1^2}$ and $\overline{u_1T'}$

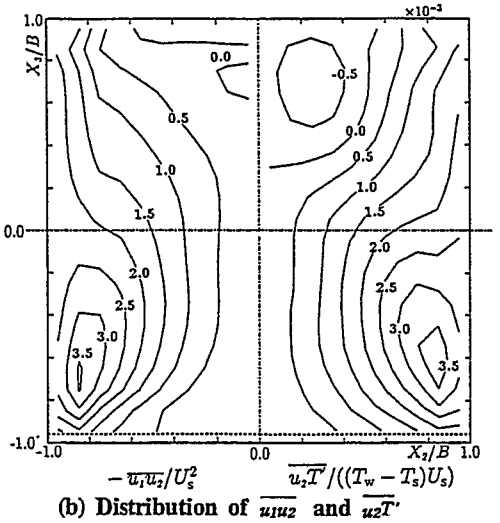

(b) Distribution of $\overline{u_1u_2}$ and $\overline{u_2T'}$

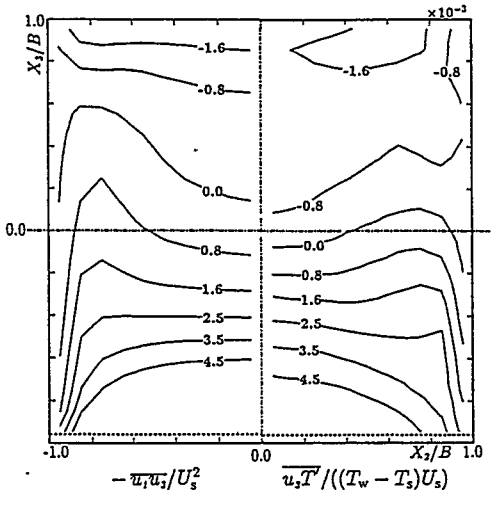

(c) Distribution of $\overline{u_1u_3}$ and $\overline{u_3T'}$

Fig.10 Distribution of turbulent heat fluxes and Reynolds stresses

observed in both results. The distributions of both results are partly similar each other, although difference between profiles of zero line for the turbulent heat flux and that for Reynolds stress is recognized. As shown in Fig.10(c), the weak similarity of distribution between the turbulent heat flux $\overline{u_3T'}$ and Reynolds stress $\overline{u_1u_3}$ seems to be also observed as well as the other two cases.

CONCLUSIONS

A numerical analysis of heat transfer has been performed for fully developed turbulent flow in a straight square duct with one roughened wall by using algebraic Reynolds stress model and turbulent heat flux model. The present method can predict well a large eddy caused by the secondary flow of the second kind in a half cross section and a small eddy, that is not measured in the experiment, is observed in the upper wall corner region in the calculation.

The distorted contour lines of axial mean velocity and temperature in the upper region of square duct by the secondary flow are predicted well by means of the present method. Adding to this, the calculated distributions of the wall shear stress and the wall heat flux are in good agreement with the experiment. On the contrary to this agreement, the present method underestimates the value of Nusselt number over the top and side smooth wall. In this numerical analysis, the similarity between the distribution of temperature and that of axial mean velocity over the top smooth wall is not observed so strongly as the experimental data, while the similarity between these two parameters over the rough wall side is not recognized as well as the experimental data. Additionally, the present method shows that the weak similarity between the distribution of Reynolds stresses and that of turbulent heat fluxes is recognized.

REFERENCES

Champagne,F.H., Harris,V.G. and Corrsin,S.,1970, "Experiments on Nearly Homogeneous Turbulent Shear Flow",J.Fluid Mech.,Vol.41,pp.81–139

Chou,P.Y.,1945,"On Velocity Correlations and the Solutions of the Equations of Turbulent Fluctuation", Quart.Appl.Math.3, pp.38–54.

Demuren,A.O. and Rodi,W.,1984,"Calculation of Turbulent-driven Secondary Motion in Non-circular Ducts",J.Fluid.Mech., Vol.140,pp.189–222

Fujita,H.,Yokosawa,H.,Hirota,M. and Nishigaki,S.,1986,"Fully Developed Turbulent Flow in a Square Duct with a Rough Wall",Trans.Jpn.Soc.Mech.Eng.,(in Japanese),Vol.53,No.492,pp. 2370–2376

Fujita,H.,Yokosawa,H.,Hirota,M. and Nagata,C.,1988,"Fully Developed Turbulent Flow and Heat Transfer in a Square Duct with Two Roughened Facing Walls",Chem.Eng.Comm.,Vol.74, pp.95–110

Fujita,H.,Yokosawa,H. and Hirota,M.,1989,"Secondary Flow of the Second Kind in Rectangular Ducts with One Rough Wall", Experimental Thermal and Fluid Science,pp.72–80

Hanjalic,K and Launder,B.E.,1972,"A Reynolds Stress Turbulence and its Application to Thin Shear Flows",J.Fluid Mech., Vol.52,pp.609–638

Harris,V.G.,Graham,J.A.H. and Corrsin,S.,1977,"Further Experiments in Nearly Homogeneous Turbulent Shear Flow",J. Fluid Mech.,Vol.81,pp.657–687

Hinze,J.O.,1973,"Experimental Investigation of Secondary Currents in the Turbulent Flow Through a Straight Conduit", Appl.Sci.Res.,Vol.28,pp.453–465

Hirota,M.,Fujita,H.,Yokosawa,H.,Kagami,S., and Murofushi, T.,1992,"Forced Convection Heat Transfer for Turbulent Flow in a Square Duct with a Rough Wall",Trans.Jpn.Soc.Mech. Eng.,(in Japanese),Vol.58,No.548,pp.1200–1208

Humphrey,J.A.C. and Whitelaw,J.H,1980,"Turbulent Flow in a Duct with Roughness",Turbulent shear flows 2,pp.174–188

Launder,B.E. and Ying,W.M.,1972, "Secondary Flows in Ducts of Square Cross-section",J.Fluid Mech.,Vol.54,pp.289–295

Launder,B.E. and Ying,W.M.,1973,"Prediction of Flow and Heat Transfer in Ducts of Square Cross-section",Heat and Fluid Flow,Vol.3,pp.115–121

Launder,B.E., Reece,G.J. and Rodi,W.,1975,"Progress in the Development of a Reynolds Stress Turbulence Closure",J.Fluid Mech.,Vol.68,pp.537–566

Launder,B.E.,1975,"On the Effects of a Gravitational Field on the Turbulent Transport of Heat and Momentum",J.Fluid Mech.,Vol.67,pp.569–581

Lumley,J.L.,1975,Lecture Series No.76,von Karman Inst., Belgium.

Rodi,W.,1976,"A New Algebraic Relation for Calculating the Reynolds Stresses",Z.Angew.Math.Mech.,56,pp.T219-T221

Sugiyama,H., Akiyama,M. and Serizawa,T.,1991,"Numerical Analysis of Developing Flow in a Square Duct Using Reynolds Stress Model",Proc.of the ASME/JSME Thermal Eng.Joint Conf.,Vol.3,pp.159–165

Sugiyama,H.,Akiyama.M.,Matsumoto.M.,Hirata.M. and Ninomiya, N.,1993,"Numerical Analysis of Fully Developed Turbulent Flow in a Square Duct with Two Facing Roughened Walls",Computational Fluid Dynamics Journal,Vol.2,No.3, pp. 319–338

Yokosawa,H.,Fujita,H.,Hirota,M. and Iwata,S.,1989, "Measurement of Turbulent Flow in a Square Duct with Roughened Walls on Two Opposite Sides",Int.J.Heat and Fluid Flow,Vol. 10,No.2,pp.125–130